CHALMERS

FINITE ELEMENT CENTER

PREPRINT 2005–07

Modeling of resistive wall mode and its control in experiments and ITER

Yueqiang Liu, M.S. Chu, A.M. Garofalo, Y. Gribov, M. Gryaznevich, T.C. Hender, D.F. Howell, R.J. La Haye, M. Okabayashi, S.D. Pinches, H. Reimerdes, P. de Vries, and EFDA-JET contributors

Chalmers Finite Element Center
CHALMERS UNIVERSITY OF TECHNOLOGY
Göteborg Sweden 2005

CHALMERS FINITE ELEMENT CENTER

Preprint 2005–07

Modeling of resistive wall mode and its control in experiments and ITER

Yueqiang Liu, M.S. Chu, A.M. Garofalo, Y. Gribov, M. Gryaznevich, T.C. Hender, D.F. Howell, R.J. La Haye, M. Okabayashi, S.D. Pinches, H. Reimerdes, P. de Vries, and EFDA-JET contributors

CHALMERS

Chalmers Finite Element Center
Chalmers University of Technology
SE–412 96 Göteborg Sweden
Göteborg, December 2005

Modeling of resistive wall mode and its control in experiments and ITER

Yueqiang Liu, M.S. Chu, A.M. Garofalo, Y. Gribov, M. Gryaznevich, T.C. Hender, D.F. Howell, R.J. La Haye, M. Okabayashi, S.D. Pinches, H. Reimerdes, P. de Vries, and EFDA-JET contributors

NO 2005–07
ISSN 1404–4382

Chalmers Finite Element Center
Chalmers University of Technology
SE–412 96 Göteborg
Sweden
Telephone: +46 (0)31 772 1000
Fax: +46 (0)31 772 3595
www.phi.chalmers.se

Printed in Sweden
Chalmers University of Technology
Göteborg, Sweden 2005

MODELING OF RESISTIVE WALL MODE AND ITS CONTROL IN EXPERIMENTS AND ITER

YUEQIANG LIU, M.S. CHU, A.M. GAROFALO, Y. GRIBOV, M. GRYAZNEVICH, T.C. HENDER, D.F. HOWELL, R.J. LA HAYE, M. OKABAYASHI, S.D. PINCHES, H. REIMERDES, P. DE VRIES, AND EFDA-JET CONTRIBUTORS AND MATS G. LARSON

Abstract. Active control of the resistive wall mode (RWM) for DIII-D [Luxon and Davis, Fusion Technol. 8, 441(1985)] plasmas is studied using the MARS-F code [Y.Q. Liu, *et al.*, Phys. Plasmas **7**, 3681(2000)]. Control optimization shows that the mode can be stabilized up to the ideal wall beta limit, using the internal control coils (I-coils) and poloidal sensors located at the outboard midplane, in combination with an ideal amplifier. With the present DIII-D power supply model, the stabilization is achieved up to 70% of the range between no-wall and ideal-wall limits. Reasonably good quantitative agreement is achieved between MARS-F simulations and experiments on DIII-D and JET (Joint European Torus) [P.H. Rebut *et al.*, Nucl. Fusion 25, 1011(1985)] on critical rotation for the mode stabilization. Dynamics of rotationally stabilized plasmas is well described by a *single* mode approximation; whilst a strongly unstable plasma requires a *multiple* mode description. For ITER [R. Aymar, P. Barabaschi, and Y. Shimomura, Plasma Phys. Controlled Fusion 44, 519(2002)], the MARS-F simulations show the plasma rotation may not provide a robust mechanism for the RWM stabilization in the advanced scenario. With the assumption of ideal amplifiers, and using optimally tuned controllers and sensor signals, the present feedback coil design in ITER allows stabilization of the $n = 1$ RWM for plasma pressures up to 80% of the range between the no-wall and ideal-wall limits.

1. Introduction

Advanced tokamaks are economically attractive fusion devices, which aim at steady state operation with a high plasma pressure and a large fraction of bootstrap current [1]. One of the good features of advanced tokamaks is that the micro-instabilities in the plasma core region are well damped, which leads to internal transport barriers, and thus improved plasma energy confinement. Moreover, it is expected that in advanced scenarios with low or reversed magnetic shear,

Date: December 16, 2005.

Key words and phrases. fusion, resistive wall mode, active control, MARS-F code.

Yueqiang Liu, Department of Applied Mechanics, Chalmers University of Technology, S–412 96 Göteborg, Sweden, *email*: yueqiang.liu@chalmers.se

M.S. Chu, A.M. Garofalo and R.J. La Haye, General Atomics, San Diego, CA, USA

Y. Gribov, Physics Unit, ITER Naka Joint Work Site, Naka, Ibaraki, Japan

M. Gryaznevich, T.C. Hender, D.F. Howell and P. de Vries, Euratom/UKAEA Fusion Association, Culham Science Centre, Abingdon, Oxon, OX14 3DB, UK

M. Okabayashi, Princeton Plasma Physics Laboratory, Princeton, New Jersey, USA

S.D. Pinches, Max-Planck-Institute for Plasmaphysik, EURATOM-Association, Garching, Germany

H. Reimerdes, Columbia University, New York, New York, USA.

neoclassical tearing modes, that are a very dangerous magnetohydrodynamic (MHD) instabilities for long pulse operations for present tokamaks and possibly for ITER, can actually be suppressed. On the other hand, it is known that the product of the plasma pressure, $\beta = 2\mu_0\langle p\rangle/\langle B^2\rangle$, and the bootstrap current fraction, $f_{\mathrm{bs}} = I_{\mathrm{bs}}/I_{\mathrm{p}}$, (where p is the plasma kinetic pressure, B the total magnetic field, $\langle\cdots\rangle$ defined as the average over plasma volume, I_{bs} the bootstrap current, I_{p} total plasma current) has an upper limit [2]

$$\beta f_{\mathrm{bs}} \lesssim 0.1(1+\kappa^2)(a/R)^{1/2}\beta_N^2,$$

where $\beta_N = \beta(\%)a(m)B_0(T)/I_p(MA)$ is the normalized beta. For advanced scenarios such as the ITER Scenario-4 [3], with conventional plasma aspect ratio $R/a \simeq 3$, and moderate plasma elongation $\kappa < 2$, improvement of the fusion performance requires maximizing β_N. However, rather broad current profiles and highly peaked pressures, typical for advanced plasmas, lead to relatively low pressure limits due to the instability of long-wavelength (low toroidal mode number n) ideal MHD kink modes. These pressure-driven, external kink instabilities can in principle be suppressed by a closely fitted conducting wall surrounding the plasma. In practice, however, walls have finite resistivity. On the time-scale over which eddy currents in the wall decay resistively, the magnetic perturbations of external modes penetrate the wall, and the stabilization is lost [4]. The resulting slow-growing, resistive wall modes (RWM) need to be stabilized to achieve high β_N in steady state operations. It is predicted that, for the ITER advanced scenario, β_N can be increased from about 2.5 up to 3.5 or even more, provided the $n = 1$ RWM is stabilized [5].

Two possible ways have been suggested to stabilize the low n RWM in a tokamak. The simple way is to rely passively on the plasma rotation. Both toroidal theory [6, 7] and experiments in DIII-D [8, 9, 10] and JET (Joint European Torus) [11] show that a high-speed toroidal rotation, typically a few percent of the Alfvén speed at the plasma center, is required for complete stabilization of the mode. One of the key physics issues is understanding of the damping mechanisms on the RWM due to the nonlinear interaction between the mode and the (stable) waves and particles in the plasma.

Another way, first proposed by Bishop [12], exploits active control. This technique is similar to the routinely used vertical control for elongated plasmas [13]. Feedback control of the RWM has been carried out in DIII-D [14, 15, 16, 17, 18], HBT-EP (High Beta Tokamak-Extended Pulse) [19], as well as in EXTRAP T2R reversed field pinch [20, 21], with very encouraging results. Theoretically, a circuit model [22], cylindrical models [23, 24, 25, 26, 27], and toroidal models [28, 29, 30, 31, 32, 33] have been developed to study feedback stabilization of the RWM. One of the key understandings is that sensors, measuring the poloidal component of the magnetic field perturbations just inside the vacuum vessel, gives superior control performance to sensors measuring the radial fields [29].

Recent experiments in DIII-D show very efficient stabilization by using internal control coils (I-coils), installed inside the vacuum vessel and above/below the midplane on the large major radius side of the torus [18]. This paper reports the feedback simulation results for DIII-D plasmas using I-coils. Also, a feedback study is made for ITER plasmas in advanced scenarios.

One way to understand the RWM damping is to compare the experimental data with numerical simulations with various damping models. Two types of experimental data are well documented:

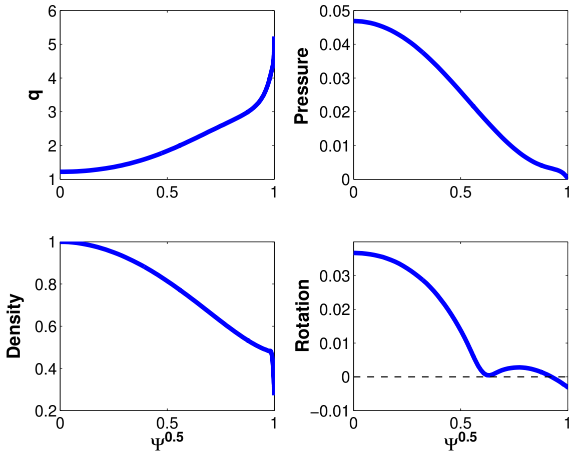

FIGURE 1. An equilibrium reconstructed from DIII-D shot 114340 at 1450ms. Shown are the profiles for the safety factor q, plasma pressure (normalized by the toroidal magnetic field pressure) and density (normalized at the plasma center), and the toroidal plasma rotation frequency (normalized by the Alfvén frequency). Ψ is the normalized poloidal magnetic flux.

the critical rotation frequency required for marginal stabilization of the RWM, and the amplitude and phase of the plasma response to an externally applied resonant field (resonant field amplification, RFA [34]). This paper reports both types of simulations using the MARS-F code [29], and compares with experiments in DIII-D and JET.

MARS-F is a linear MHD stability code developed from the MARS code [35, 36], with added features such as feedback [28] and the kinetic damping model [37]. The latter is based on a simplified drift-kinetic large-aspect-ratio analysis [38]. Besides the Alfvén continuum damping, a parallel viscous force [36] is also introduced in the code in order to model the sound wave damping.

Section II of this paper reports the feedback simulations for DIII-D plasmas using I-coils. Section III gives ITER predictions for active control of the RWM. Section IV compares the MARS-F computed critical rotation with the recent experiments on DIII-D and JET, and gives predictions for ITER. Section V discusses modeling issues of the plasma response for the resonant field amplification. The work is summarized in Section VI.

2. Feedback study for DIII-D

To simulate the feedback experiments on DIII-D, we choose a plasma equilibrium reconstructed from the shot 114340 at 1450ms. The profiles for the safety factor q, the plasma pressure and density, as well as the plasma toroidal rotation are shown in Fig. 1. For this shot, the plasma rotation is kept very slow in a large outer region of the plasma. The resistive wall mode is *not* stabilized by the plasma rotation. Feedback control, using internal coils (I-coils), keeps the mode stable for more than 50 ms at low rotation [18].

2.1. Computing plasma response model. In the simulation, we neglect the plasma rotation. Using the MARS-F code, we compute the plasma response model, defined as a frequency dependent transfer function [39]

$$P = \frac{\psi_s}{M_{sf} I_f}, \tag{2.1}$$

where ψ_s is the magnetic flux detected by poloidal sensors located at the outboard midplane just inside the DIII-D vacuum vessel. M_{sf} is a normalization factor, chosen as the *radial* field produced at the sensor position by 1A current flowing in the I-coils in free space. The feedback current is denoted as I_f. The open-loop response P is usually well approximated by a low order rational function (Padé approximation) [28].

We compute transfer functions P_U and P_L for both sets of I-coils above and below the midplane, respectively. The poloidal sensors at the midplane is used for both sets of I-coils. Assuming the sensor signal is fed back to two sets of I-coils via the same controller K, and with opposite toroidal phase shift $\pm\phi_P$ (the total phasing between the upper and lower coil sets becomes $2\phi_P$), the total transfer function is

$$P = P_U \exp(j\phi_P) + P_L \exp(-j\phi_P),$$

where j is the imaginary unit.

2.2. Control optimization. The control optimization is performed, that (1) gives stabilization of the RWM, (2) meets certain prescribed criteria on the control performance. We assume a simple PD-controller with proportional (P) and derivative (D) actions

$$K(s) = K_p \frac{1 + T_d s}{1 + T_d s/\xi},$$

where s is the Laplace variable. K_p is the proportional gain, generally chosen as a complex number with phase ϕ_K. [ϕ_K corresponds to a toroidal phase shift between the control signal and the sensor signal.] T_d (real number) is the derivative gain. An additional parameter $\xi > 1$ is chosen to prevent unphysical behavior at very high frequencies. The control performance is measured by control activity $||KS||_\infty$ and sensitivity $||S||_\infty$ [40]

$$S(j\omega) = \frac{1}{1 + K(j\omega)P(j\omega)}, \quad ||KS||_\infty = \sup_\omega |K(j\omega)S(j\omega)|, \quad ||S||_\infty = \sup_\omega |S(j\omega)|,$$

where ω is the real frequency belonging to a chosen frequency band. In the control optimization, we minimize the control activity $||KS||_\infty$ while applying constraints on the sensitivity $||S||_\infty \leq 2.0$. Three strategies are tested with respect to the choice of the optimization variables c:
(1) $c = \{K_p, T_d, \xi\}$, where K_p is real (i.e. $\phi_K = 0$), fix $\phi_P = 150^o$,
(2) $c = \{K_p, T_d, \xi, \phi_P\}$, fix $\phi_K = 0$,
(3) $c = \{K_p, T_d, \xi, \phi_P\}$, where K_p is complex (i.e. also optimize ϕ_K).

We perform a control study for both ideal power amplifiers (with zero time delay and infinite bandwidth) and the DIII-D experimental amplifiers.

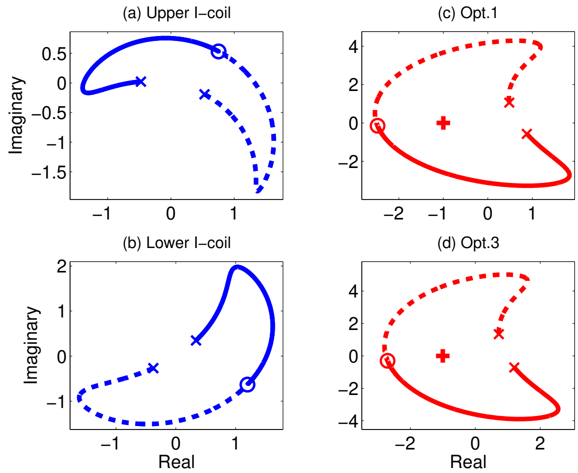

FIGURE 2. Transfer functions plotted on the complex plane, for real frequencies $-10^3 \leq \omega\tau_w \leq 10^3$. Solid (dashed) line denotes positive (negative) ω. 'o' denotes $\omega = 0$, and 'x' denotes $|\omega\tau_w| = 10^3$. Shown a case for the plasma close to the ideal wall beta limit with $C_\beta = 0.9$. An ideal amplifier is assumed. (a) Plasma response to the internal control coils (I-coils) above the midplane. (b) Plasma response to the I-coils below the midplane. (c) Plasma response to both sets of I-coils connected to the same optimal PD controller with *real* feedback gains. Toroidal phase difference between upper and lower sets is 300°. (d) Plasma response to both sets of I-coils connected to the same optimal PD controller with *complex* feedback gains. Both toroidal phasings of feedback gains and I-coil sets are also optimized.

2.3. **Control with Ideal amplifier.** Figure 2 shows the control results for a plasma close to the ideal wall limit at $C_\beta \equiv (\beta - \beta^{no-wall})/(\beta^{ideal-wall} - \beta^{no-wall}) = 0.9$. The instability of the RWM and the possibility of its feedback control is usually well correlated to the parameter C_β. Figures 2(a) and (b) show, in the complex plane, the computed transfer function $P_U(j\omega)$ and $P_L(j\omega)$, with real frequencies (normalized by the wall time) $\omega\tau_w \in [-10^3, 10^3]$. Figure 2(c) shows the transfer function $K(j\omega)P(j\omega)$ for the optimal controller K according to the optimization strategy (1). The corresponding result for the optimization strategy (3) is shown in Fig. 2(d).

According to the Cauchy principle of phase variation, the closed loop is stable if the Nyquist curves, shown in Fig. 2, encircle -1 once in the counter clock-wise direction, as the frequency ω varies from $-\infty$ to $+\infty$. In our case, both closed-loops from Fig. 2(c) and (d) are stable, with rather good stability margin. [A quantitative measure of the stability margin is the sensitivity $||S||_\infty$. The shortest distance between -1 and the Nyquist curve for $K(j\omega)P(j\omega)$ is equal to $1/||S||_\infty$, since according to the definition, $1/\max|S(j\omega)| = \min|1 + K(j\omega)P(j\omega)|$.]

The similarity of Figures 2(c) and (d) indicates that the *ad-hoc* choice of $\phi_P = 150°$ is close to the optimal, and feedback with real gains is good enough for this case. Indeed, the quantitative measures of the control activity $||KS||_\infty$ and sensitivity $||S||_\infty$ are quite close, as shown in Fig. 3,

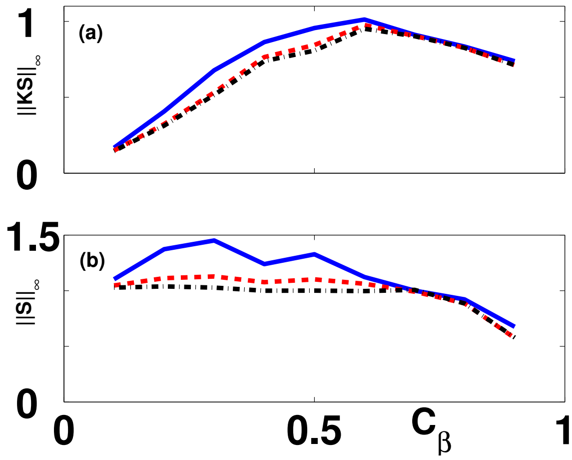

FIGURE 3. Optimal control results with ideal amplifiers. Solid curves correspond to real feedback gains and fixed toroidal phasing at 300° between upper and lower I-coil sets. Dashed curves correspond to real gains and optimal phasing for I-coils. Dash-dotted curves correspond to optimal phasing for both complex gains and I-coil sets. Shown are (a) the optimal control activity $||KS||_\infty$, and (b) the achieved stability margin $||S||_\infty$, versus the plasma pressure C_β. Controller optimization is made for each C_β individually.

for all three optimization strategies. The control optimization is made individually for each C_β value. We conclude also that, with an ideal amplifier, the I-coils can provide full stabilization of the RWM up to the ideal wall beta limit, with good performance.

The optimal controller gains K_p and T_d are shown in Fig. 4(a) and (b), respectively. The optimal value for parameter ξ is generally much larger than unity. We note that the derivative action is almost not required. The phase angles ϕ_K and ϕ_P are shown in Fig. 5(a) and (b), respectively. The optimal phasing between two sets of I-coils can be as low as 240° at low pressure. The fact that the optimal control results are only slightly better than the ad-hoc choice of 300° indicates, that the control is not very sensitive to the choice of ϕ_P.

2.4. **Control with DIII-D amplifier.** We use the following transfer function to specify the DIII-D switching power amplifiers, which were installed in 2000 [41]

$$P_a(s) = \frac{\Omega_1}{s+\Omega_1} \times \frac{\Omega_2}{s+\Omega_2} \times \exp(-s\tau_d),$$

where $\Omega_1 = 5373 - 8205j\text{sec}^{-1}$, $\Omega_2 = 2692 + 960j\text{sec}^{-1}$, $\tau_d = 65\mu\text{s}$.

The total open-loop transfer function $P(s)$ is now replaced by $P(s)P_a(s)$. We perform again the control optimization for all C_β. Figure 6 shows the results for $C_\beta = 0.7$ in Nyquist diagrams. At this plasma pressure, the optimal controller can marginally stabilize the mode, with rather poor performance. No optimal controller is found at $C_\beta = 0.8$ that can still stabilize the mode.

Figure 7 shows the optimal control results for varying plasma pressures. At $C_\beta > 0.3$, the control performance specification $||S||_\infty \leq 2.0$ can no longer be satisfied, as shown in Fig. 7(b).

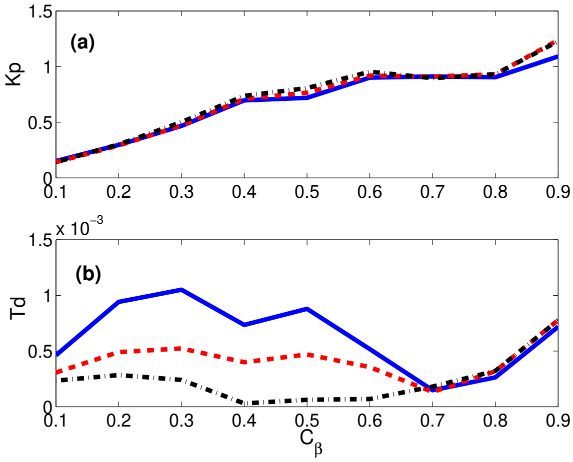

FIGURE 4. The same cases as in Fig. 3. Shown are optimal controller gains (amplitude) for (a) proportional action K_p, and (b) derivative action T_d.

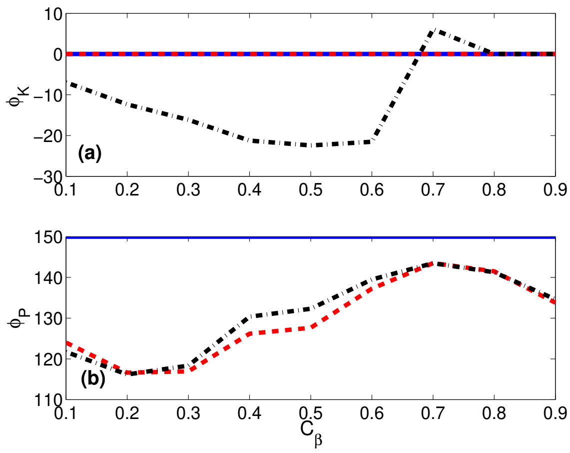

FIGURE 5. The same cases as in Fig. 3. Shown are (a) toroidal phasings (in degrees) for optimal feedback gains, and (b) half of toroidal phasing (in degrees) between upper and lower sets of I-coils.

The optimal control gains are shown in Fig. 8(a-b). Larger derivative gains (about 10% of the proportional gain) are generally required in order to compensate the phase delay caused by the power supply. The optimal phase angles for ϕ_K and ϕ_P varies with varying plasma pressure (Fig. 9), which does not lead to significant variation of the control results.

3. Feedback study for ITER

We also studied active control of the $n = 1$ RWM for the ITER steady state scenario (Scenario-4) [3, 5]. This scenario has weak negative magnetic shear and a highly shaped plasma. The total plasma current is 9MA, with about 340MW fusion power production at $Q = 5$. The design

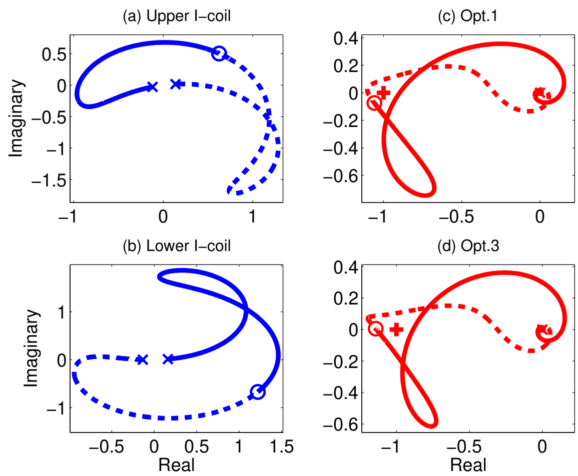

FIGURE 6. A similar study to Fig. 2, with the plasma pressure at $C_\beta = 0.7$. A realistic power supply model from DIII-D experiments is included in the control optimization.

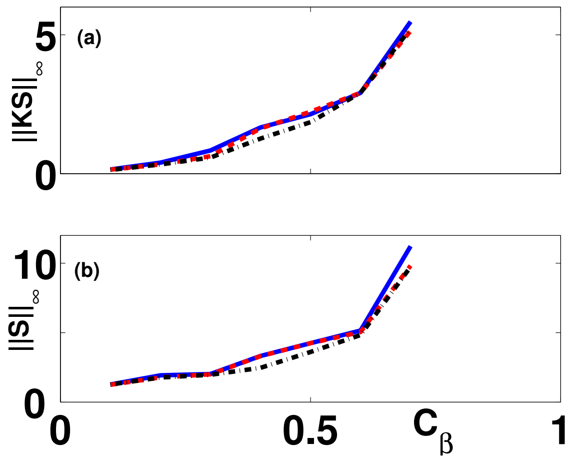

FIGURE 7. Optimal control results with the DIII-D amplifier. The curves notation follows Fig. 3.

plasma is marginally unstable without the wall. We scaled the plasma pressure up to the ideal-wall limit for the inner wall, keeping the total plasma current at 9MA.

The side correction coils have been used for the RWM feedback control. These are superconducting coils, located along the outboard midplane and external to the ITER walls (at a radial distance of about $3a$, where a the plasma minor radius), with three pairs of toroidally opposite coils connected to produce the $n = 1$ magnetic field.

Using internal poloidal sensors and assuming an ideal amplifier, MARS-F calculations have shown that the present design of feedback coils allow stabilization of the $n = 1$ RWM up to $C_\beta \simeq 60\%$ with proportional actions alone. Better results can be achieved by using optimally

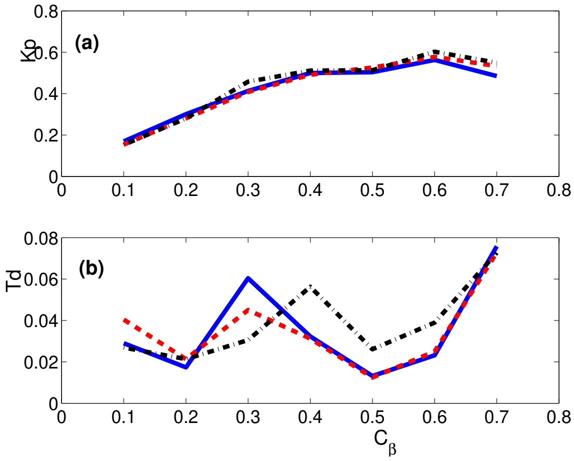

FIGURE 8. Optimal controller obtained assuming the DIII-D amplifier. Notations are the same as in Fig. 4.

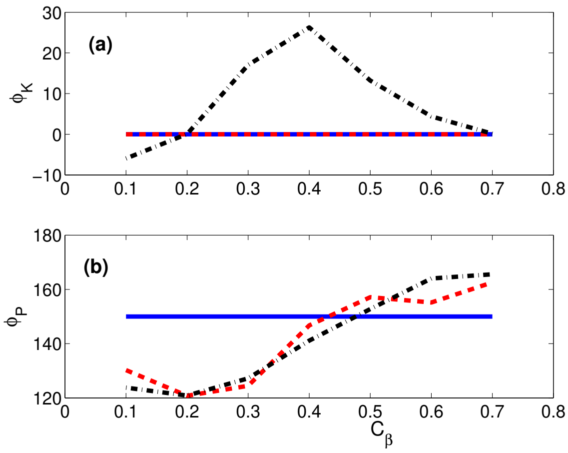

FIGURE 9. Optimal toroidal phasings assuming the DIII-D amplifier. Notations are the same as in Fig. 5.

tuned PID (proportional, integral and derivative) controllers and improved sensor signals. We have optimized the PID gains to achieve the minimum peak voltage for a reference event, where the controller is turned on after the field reaches 1.5 mT.

In Ref. [37], we have shown that, with the design voltage limit of 300 V/turn for the amplifier, the RWM can be controlled with good performance ($||S||_\infty = 2$) for $C_\beta \lesssim 65\%$, and with moderate performance ($||S||_\infty = 2.5$) for $C_\beta \lesssim 70\%$. The peak voltage is further reduced if we use internal poloidal sensor signals compensated by an optimally chosen signal. The RWM can be stabilized, with good performance, up to $C_\beta \gtrsim 80\%$.

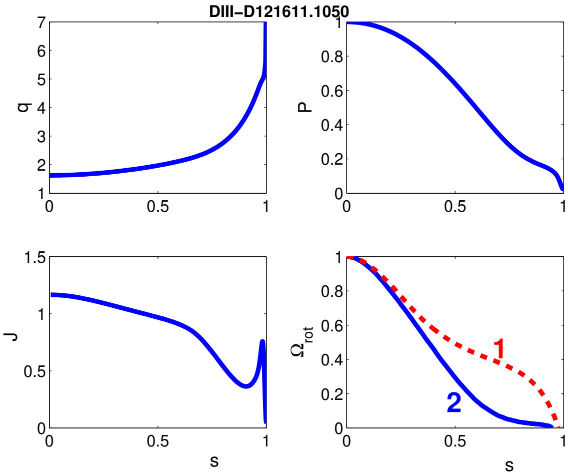

FIGURE 10. Equilibrium profiles reconstructed for the DIII-D shot 121611 at 1165.5ms, for the safety factor q, plasma pressure P (normalized at the plasma center) and surface averaged current density J (normalized by $B_0/(\mu_0 R_0)$, where B_0 is the toroidal vacuum field, R_0 the major radius, and μ_0 the vacuum permeability), and toroidal rotation $\Omega_{\rm rot}$ (normalized at the plasma center). Two rotation profiles are considered: before applying the external field (dashed curve) and after the magnetic braking (solid curve), when the critical rotation is measured.

4. Critical rotation for RWM stabilization

4.1. **Simulations for DIII-D.** On DIII-D, the critical rotation, required for stabilization of the RWM, is measured by applying an external error magnetic field to gradually slow the plasma rotation. One example is the shot 121611, which is part of a DIII-D/JET comparison of RWM physics [42]. Figure 10 shows the equilibrium profiles reconstructed at high beta shortly before the onset of the RWM. The rotation profile (normalized at the plasma center) at this moment is shown as solid line. Shown also is the rotation profile measured before applying the external field (dashed line), when the plasma is stabilized by the rotation.

The MARS-F computed critical rotation (evaluated at the plasma center) is shown in Fig. 11, for both rotation profiles. The kinetic damping model is assumed. The computed critical rotation with magnetic braking (profile 2) is close to the experimental value, as shown by the solid line. The computed critical rotation at the plasma center is reduced by about 40% for the case without magnetic braking (profile 1). This comparison shows that the critical rotation, as defined at the plasma center, is sensitive to the rotation profile.

We also compute the critical rotation for the equilibrium that was used in the feedback study described in Section II. The equilibrium and rotation profiles are shown in Fig. 1. In Fig. 12, we plot the ratio of the computed critical rotation to the experimental value, for increasing plasma pressures. The plasma pressure in the experiment corresponds to C_β about 0.35. The RWM at this pressure is predicted to be unstable, which confirms the experimental observations.

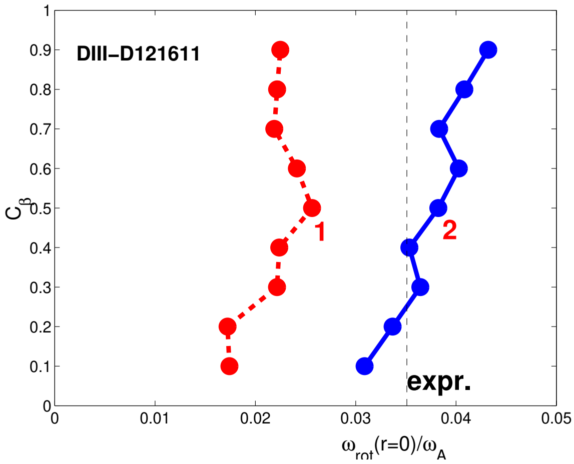

FIGURE 11. Computed critical rotation versus the plasma pressure C_β, for both rotation profiles shown in Fig. 10. The kinetic damping model is used in MARS-F calculations. Shown also the critical rotation measured in the magnetic braking experiment.

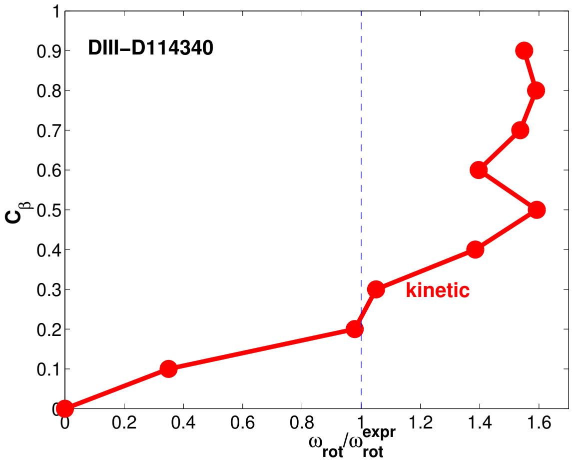

FIGURE 12. Computed critical rotation versus the plasma pressure C_β for the DIII-D shot 114340. The equilibrium and rotation profiles are shown in Fig. 1.

4.2. **Simulations for JET.** Figure 13 shows comparison of the MARS-F computed critical rotation against the experimental data on JET. The calculations assume either parallel sound wave damping (dashed curves), with various values for adjustable damping coefficient $\kappa_{||}$, or the kinetic damping (solid curve). A series of JET equilibria, reconstructed from JET shot 62366, has been used in calculations [37]. The kinetic damping gives quantitatively correct predictions for the critical rotation.

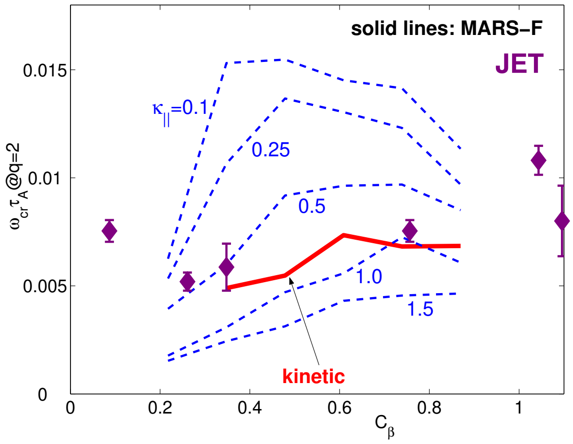

FIGURE 13. The critical rotation frequency at the $q = 2$ surface, normalized by Alfvén frequency, versus the plasma pressure C_β. Plotted are JET experimental data (dots) and the MARS-F results with parallel sound wave damping (dashed curves) and semi-kinetic damping (solid curve) models.

4.3. **The q_{95} scaling.** Using the kinetic damping model, it has been computed in Ref. [37], that the critical rotation, measured at the plasma center, decreases with increasing q_{95}. The dependence follows an approximate scaling as $1/q_{95}^2$ as shown in Fig. 14. In the same Figure, we also plot the critical rotation at the $q = 2$ surface versus q_{95}. No explicit dependence is seen. Both observations are also made in experiments in DIII-D, JET and NSTX [42]. One possible explanation for this is the variation of rotation profiles between different machines, as shown in Fig. 15. [For a similar q-profile from two machines and a similar critical rotation at the $q = 2$ surface, a more strongly peaked rotation profile (in DIII-D as compared to JET, for example) could give a larger critical rotation evaluated at the plasma center.] Even with a fixed rotation profile, the dependence can be different for the critical rotation at the plasma center compared with that at the $q = 2$ surface, as shown by the computed data for DIII-D 110634 in Fig. 14. This is because increasing q_{95} shifts the $q = 2$ surface inward into the plasma, where the rotation speed is higher.

Figure 14 also shows the critical rotation predicted for the ITER advanced plasmas from Scenario-4. Transport calculations in Ref. [3] indicate that the ITER plasma rotation speed is close to the MARS-F computed critical value (less than 2% of the Alfvén speed at the plasma center). Therefore, ITER plasma rotation may not provide a robust stabilization mechanism for the RWM.

5. DYNAMICS OF STABLE RWM

The transfer function, defined in Eq. (2.1), can also be used to describe the dynamics of a stable plasma, where the RWM is stabilized by fast plasma rotation. The current I_f produces a resonant error field, that can be amplified by the stable plasma [34]. We try to establish how many poles (modes) are required to adequately represent the plasma response.

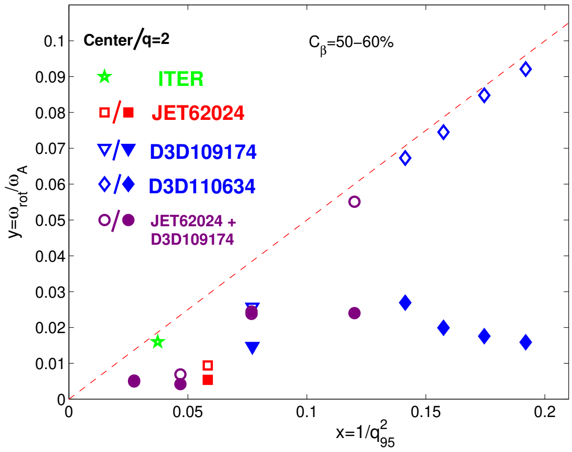

FIGURE 14. The q_{95} scan of the *computed* critical rotation frequency $\omega_{\rm rot}$, normalized by the Alfvén frequency ω_A, for various equilibria. The plasma pressure is kept approximately the same in terms of C_β (=50-60%). The critical rotation frequencies are defined both at the plasma center (open symbols) and at the $q=2$ surface (filled symbol).

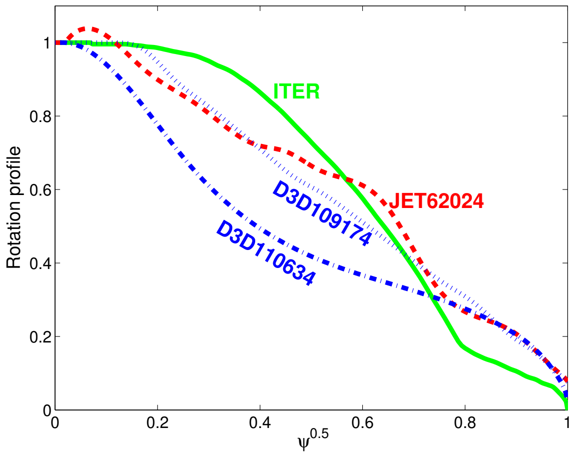

FIGURE 15. The rotation profiles (normalized by the central value) used in the calculations in Fig. 14 for various equilibria. The rotation profile for ITER is predicted by transport calculations [3].

We choose a test toroidal equilibrium with the JET-like shape, and compute the plasma response with various rotation speeds. The RWM for the chosen equilibrium (with the plasma pressure β_N at the middle between the no-wall and the ideal-wall limits) is stabilized by a critical rotation $\omega_{\rm rot}^{\rm cr}/\omega_A = 0.017$ at the plasma center. Figure 16 shows the Nyquist plot for the plasma response for four rotation speeds: $\omega_{\rm rot}/\omega_A = 0.0, 0.01, 0.03, 0.06$. In the first two cases (solid

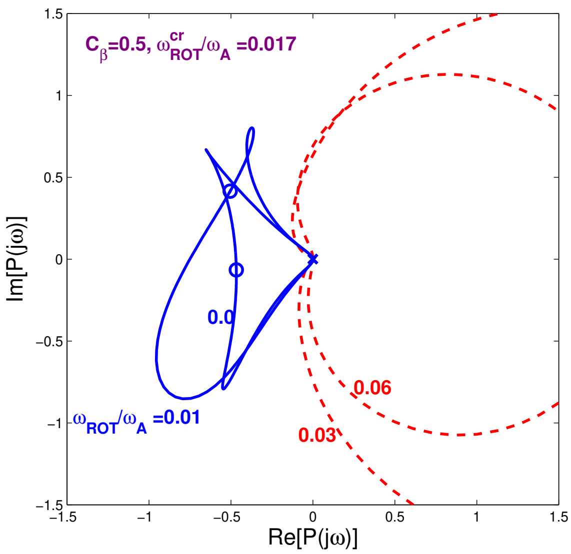

FIGURE 16. Nyquist plot of transfer functions for both unstable (solid curves) and stable (dashed curves) plasma response. A test toroidal equilibrium with JET-like shape and $C_\beta = 0.5$ is considered. The RWM is unstable at low plasma rotation and eventually stabilized by a rotation frequency larger than $0.017\omega_A$ at the plasma center.

curves), the plasma is *unstable*. A minimum of 3 poles are required to reach a good approximation of the plasma response computed by the MARS-F. The Nyquist curves for the last two cases (dashed), where the plasma is *stable*, are very close to circles. Such a response is well described by a single pole transfer function.

As an example, the plasma response at $\omega_{\rm rot}/\omega_A = 0.01$ is well approximated by a transfer function

$$P(s) = \frac{1.5046+0.1124j}{s-1.3586-0.7745j} + \frac{1.3205+0.4451j}{s+1.4399+0.1298j} + \frac{-2.1849-0.5422j}{s+3.6456-0.4760j}.$$

Figure 17(a) shows the three poles in the complex plane, together with the growth rates (filled 'o') of the unstable RWM with increasing the rotation frequency, as well as the damping rates ('x') of the stable RWM at no rotation. The unstable pole coincides with the growth rate of the unstable RWM. The two stable poles lump the contribution from all the stable RWMs. Note that these two stable poles are located close to the origin, giving a significant contribution to the total plasma response.

At $\omega_{\rm rot}/\omega_A = 0.03$, the plasma is stable. We obtain the following function by including two poles

$$P(s) = \frac{1.8283-0.1822j}{s+0.5530-0.7080j} + \frac{-1.2261-0.4807j}{s+6.2110+4.3657j}.$$

The poles are plotted in Fig. 17(b), together with the growth/damping rates of the RWM computed by MARS-F. Note that the first stable pole corresponds to the damping rate of the RWM

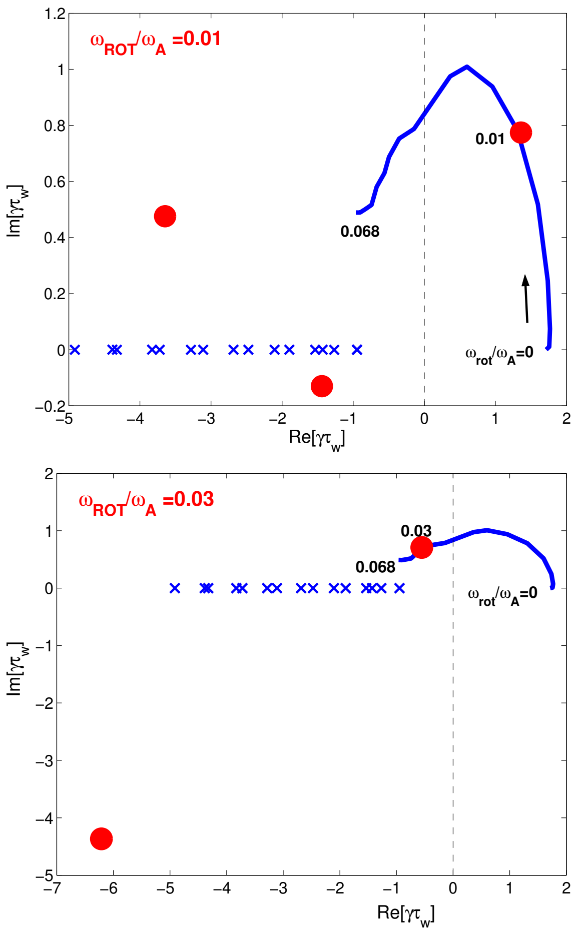

FIGURE 17. Poles (filled 'o') in the rational function approximation for the *unstable (stable)* plasma response at plasma rotation $\omega_{\rm rot}/\omega_A = 0.01(0.03)$. As for a reference, shown are also growth rates (solid lines) of the unstable RWM with increasing the rotation frequency, as well as damping rates ('x') of the stable RWM at no rotation.

stabilized by the plasma rotation. The second, lumped pole is rather far from the origin, giving a minor contribution to the total plasma response. [The contribution from the second pole becomes significant only at higher frequencies out of the frequency range for the RWM.] Therefore, we conclude that a single pole can give a good approximation for the response of stable plasmas. This explains why a single mode model works well in interpreting the experimental data from the RFA experiments [43].

6. CONCLUSIONS AND DISCUSSIONS

Using the MARS-F code, feedback stabilization of the RWM is simulated for DIII-D plasmas. Control optimization has been performed based on the computed plasma response models. The

DIII-D I-coils, with outboard midplane internal poloidal sensors and *ideal amplifiers*, can provide stabilization of the RWM up to the ideal wall beta limit. With the *DIII-D switching power amplifiers*, the stabilization up to $C_\beta = 0.7$ can be achieved.

Reasonably good quantitative agreement is achieved between MARS-F simulations and experiments on DIII-D and JET, on the critical rotation for the mode stabilization. The computed q_{95} scaling is also confirmed by the experimental measurements. The kinetic damping model is an essential ingredient for achieving the agreement. Calculations for DIII-D plasmas also show that the critical rotation is sensitive to the rotation profile.

Dynamics of rotationally stabilized plasmas, the so-called resonant field amplification, is well described by a *single* mode approximation; whilst a strongly unstable plasma requires a *multiple* mode description.

According to the kinetic damping model, the ITER plasma rotation is close to the predicted critical value, and thus may not provide a robust mechanism for the RWM stabilization in the advanced Scenario 4. Active control of the mode using feedback is an alternative way to stabilize the RWM in ITER.

With the present feedback coil design for ITER, it is possible to stabilize the $n = 1$ RWM for plasma pressures up to $C_\beta = 0.8$, using optimally tuned PID controllers and optimally compensated internal poloidal sensor signals.

For more realistic prediction of the feedback performance in ITER, other issues such as 3D wall effects, system noise and the superconducting coil AC losses, need to be addressed.

Acknowledgments

This work was partly conducted under the European Fusion Development Agreement and partly funded by EURATOM, the Swedish Research Council, the UK Engineering and Physical Sciences Research Council, and the US Department of Energy. YQL gratefully acknowledge discussions with Dr. E.J. Strait during preparation of the manuscript.

References

[1] C. Kessel, J. Manickam, G. Rewoldt, and W. M. Tang, Phys. Rev. Lett. **72**, 1212(1994).
[2] A. Bondeson, D.H. Liu, F.X. Söldner, M. Persson, Yu.F. Baranov, and G.T.A. Huysmans, Nucl. Fusion **39**, 1523(1999).
[3] A. Polevoi, S.Yu. Medvedev, V.D. Pustovitov, V.S. Mukhovatov, M. Shimada, A.A. Ivanov, Yu.Yu. Poshekhonov, M.S. Chu, Fusion Energy 2002 (Proc. 19th Int. Conf. Lyon, 2002) (Vienna: IAEA) CD-ROM file CT/P-08 and http://www.iaea.org/programmes/ripc/physics/fec2002/html/fec2002.htm
[4] D. Pfirsch and H. Tasso, Nucl. Fusion **11**, 259(1971).
[5] Y.Q. Liu, A. Bondeson, Y. Gribov, and A. Polevoi, Nucl. Fusion **44**, 232(2004).
[6] A. Bondeson and D.J. Ward, Phys. Rev. Lett. **72**, 2709(1994).
[7] D. Gregoratto, A. Bondeson, M.S. Chu, and A.M. Garofalo, Plasma Phys. Controll. Fusion **43**, 1425(2001).
[8] A.M. Garofalo, A.D. Turnbull, M.E. Austin, *et al.*, Phys. Rev. Lett. **82**, 3811(1999).
[9] A.M. Garofalo, T.H. Jensen, L.C. Johnson, *et al.*, Phys. Plasmas **9**, 1997(2002).
[10] R.J. La Haye, A. Bondeson, M.S. Chu, A.M. Garofalo, Y.Q. Liu, G.A. Navratil, M. Okabayashi, H. Reimerdes and E.J. Strait, Nucl. Fusion **44**, 1197(2004).

[11] T.C. Hender, M. Gryaznevich, Y.Q. Liu, *et al.*, Fusion Energy 2004 (Proc. 20th Int. Conf. Vilamoura, 2004) (Vienna: IAEA) CD-ROM file EX/P2-22 and http://www-naweb.iaea.org/napc/physics/fec/fec2004/datasets/index.html
[12] C.M. Bishop, Plasma Phys. Controll. Fusion **31**, 1179(1989).
[13] E.A. Lazarus, J.B. Lister, G.H. Neilson, Nucl. Fusion **30**, 111(1990).
[14] E.D. Fredrickson, J. Bialek, A.M. Garofalo, *et al.*, Plasma Phys. Controll. Fusion **43**, 313(2001).
[15] A.M. Garofalo, M.S. Chu, E.D. Fredrickson, *et al.*, Nucl. Fusion **41**, 1171(2001).
[16] M. Okabayashi, J. Bialek, M.S. Chance, *et al.*, Phys. Plasmas **8**, 2071(2001).
[17] E.J. Strait, J. Bialek, N. Bogatu, *et al.*, Nucl. Fusion **43**, 430(2003).
[18] E.J. Strait, J.M. Bialek, I.N. Bogatu, *et al.*, Phys. Plasmas **11**, 2505(2004).
[19] C. Cates, M. Shilov, M.E. Mauel, G.A. Navratil, D. Maurer, S. Mukherjee, D. Nadle, J. Bialek, and A. Boozer, Phys. Plasmas **7**, 3133(2000).
[20] P.R. Brunsell, D. Yadikin, D. Gregoratto, *et al.*, Phys. Rev. Lett. **93**, 225001(2004).
[21] J.R. Drake, P.R. Brunsell, D. Yadikin, *et al.*, Nucl. Fusion **45**, 557(2005).
[22] M. Okabayashi, N. Pomphrey, R.E. Hatcher, Nucl. Fusion **38**, 1607(1998).
[23] R. Fitzpatrick, T.H. Jensen, Phys. Plasmas **3**, 2641(1996).
[24] V.D. Pustovitov, Plasma Physics Reports, **27**, 195(2001).
[25] A. Bondeson, Y.Q. Liu, D. Gregoratto, Y. Gribov, and V.D. Pustovitov, Nucl. Fusion **42**, 768(2002).
[26] J.M. Finn, Phys. Plasmas **11**, 4361(2004).
[27] A.H. Boozer, Phys. Plasmas **11**, 110(2004).
[28] Y.Q. Liu and A. Bondeson, Phys. Rev. Lett. **84**, 907(2000).
[29] Y.Q. Liu, A. Bondeson, C.M. Fransson, B. Lennartson, and C. Breitholtz, Phys. Plasmas **7**, 3681(2000).
[30] J. Bialek, A.H. Boozer, M.E. Mauel, and G.A. Navratil, Phys. Plasmas **8**, 2170(2001).
[31] M.S. Chu, M.S. Chance, A.H. Glasser and M. Okabayashi, Nucl. Fusion **43**, 441(2003).
[32] S.Yu. Medvedev and V.D. Pustovitov, Plasma Physics Reports **30**, 895(2004).
[33] Y.Q. Liu, A. Bondeson, D. Gregoratto, C.M. Fransson, Y. Gribov and R. Paccagnella, Nucl. Fusion **44**, 77(2004).
[34] A.H. Boozer, Phys. Rev. Lett. **86**, 5059(2001).
[35] A. Bondeson, G. Vlad, H. Lütjens, Phys. Fluids **B4**, 1889(1992).
[36] M.S. Chu, J.M. Greene, T.H. Jensen, R.L. Miller, A. Bondeson, R.W. Johnson, and M.E. Mauel, Phys. Plasmas **2**, 2236(1995).
[37] Y.Q. Liu, A. Bondeson, M.S. Chu, J-Y. Favez, Y. Gribov, M. Gryaznevich, T.C. Hender, D.F. Howell, R.J. La Haye, J.B. Lister, Nucl. Fusion **45**, 1131(2005).
[38] A. Bondeson and M.S. Chu, Phys. Plasmas **3**, 3013(1996).
[39] A. Bondeson, Y.Q. Liu, D. Gregoratto, C.M. Fransson, B. Lennartson, C. Breitholtz, Y. Gribov, and V.D. Pustovitov, Phys. Plasmas **9**, 2044(2002).
[40] C.M. Fransson, B. Lennartson, C. Breitholtz, A. Bondeson, and Y.Q. Liu, Phys. Plasmas **7**, 4143(2000).
[41] A.M. Garofalo, T.H. Jensen, and E.J. Strait, Phys. Plasmas **9**, 4573(2002).
[42] H. Reimerdes, T.C. Hender, D.F. Howell, *et al.*, "Cross-Machine Comparison of Resonant Field Amplification and Resistive Wall Mode Stabilization by Plasma Rotation", this Conference(2005).
[43] H. Reimerdes, M.S. Chu, A.M. Garofalo, G.L. Jackson, R.J. La Haye, G.A. Navratil, M. Okabayashi, J.T. Scoville, and E.J. Strait, Phys. Rev. Lett. **93**, 135002(2004).

CHALMERS FINITE ELEMENT CENTER PREPRINTS

2003–01 *A hybrid method for elastic waves*
Larisa Beilina

2003–02 *Application of the local nonobtuse tetrahedral refinement techniques near Fichera-like corners*
L. Beilina, S. Korotov and M. Křížek

2003–03 *Nitsche's method for coupling non-matching meshes in fluid-structure vibration problems*
Peter Hansbo and Joakim Hermansson

2003–04 *Crouzeix–Raviart and Raviart–Thomas elements for acoustic fluid–structure interaction*
Joakim Hermansson

2003–05 *Smoothing properties and approximation of time derivatives in multistep backward difference methods for linear parabolic equations*
Yubin Yan

2003–06 *Postprocessing the finite element method for semilinear parabolic problems*
Yubin Yan

2003–07 *The finite element method for a linear stochastic parabolic partial differential equation driven by additive noise*
Yubin Yan

2003–08 *A finite element method for a nonlinear stochastic parabolic equation*
Yubin Yan

2003–09 *A finite element method for the simulation of strong and weak discontinuities in elasticity*
Anita Hansbo and Peter Hansbo

2003–10 *Generalized Green's functions and the effective domain of influence*
Donald Estep, Michael Holst, and Mats G. Larson

2003–11 *Adaptive finite element/difference method for inverse elastic scattering waves*
Larisa Beilina

2003–12 *A Lagrange multiplier method for the finite element solution of elliptic domain decomposition problems using non-matching meshes*
Peter Hansbo, Carlo Lovadina, Ilaria Perugia, and Giancarlo Sangalli

2003–13 *A reduced P^1–discontinuous Galerkin method*
R. Becker, E. Burman, P. Hansbo, and M.G. Larson

2003–14 *Nitsche's method combined with space–time finite elements for ALE fluid–structure interaction problems*
Peter Hansbo, Joakim Hermansson, and Thomas Svedberg

2003–15 *Stabilized Crouzeix–Raviart element for the Darcy-Stokes problem*
Erik Burman and Peter Hansbo

2003–16 *Edge stabilization for the generalized Stokes problem: a continuous interior penalty method*
Erik Burman and Peter Hansbo

2003–17 *A conservative flux for the continuous Galerkin method based on discontinuous enrichment*
Mats G. Larson and A. Jonas Niklasson

2003–18 *CAD–to–CAE integration through automated model simplification and adaptive modelling*
K.Y. Lee, M.A. Price, C.G. Armstrong, M.G. Larson, and K. Samuelsson

2003–19 *Multi-adaptive time integration*
Anders Logg

2003–20 *Adaptive computational methods for parabolic problems*
Kenneth Eriksson, Claes Johnson, and Anders Logg

2003–21 *The FEniCS project*
T. Dupont, J. Hoffman, C. Johnson, R.C. Kirby, M.G. Larson, A. Logg, and R. Scott

2003–22 *Adaptive finite element methods for LES: Computation of the mean drag coefficient in a turbulent flow around a surface mounted cube using adaptive mesh refinement*
Johan Hoffman

2003–23 *Adaptive DNS/LES: a new agenda in CFD*
Johan Hoffman and Claes Johnson

2003–24 *Multiscale convergence and reiterated homogenization of parabolic problem*
Anders Holmbom, Nils Svanstedt, and Niklas Wellander

2003–25 *On the relationship between some weak compactnesses with different numbers of scales*
Anders Holmbom, Jeanette Silfver, Nils Svanstedt, and Niklas Wellander

2003–26 *A posteriori error estimation in computational inverse scattering*
Larisa Beilina and Claes Johnson

2004–01 *Computability and adaptivity in CFD*
Johan Hoffman och Claes Johnson

2004–02 *Interpolation estimates for piecewise smooth functions in one dimension*
Anders Logg

2004–03 *Estimates of derivatives and jumps across element boundaries for multi-adaptive Galerkin solutions of ODEs*
Anders Logg

2004–04 *Multi-adaptive Galerkin methods for ODEs III: Existence and stability*
Anders Logg

2004–05 *Multi-adaptive Galerkin methods for ODEs IV: A priori error estimates*
Anders Logg

2004–06 *A stabilized non-conforming finite element method for incompressible flow*
Erik Burman and Peter Hansbo

2004–07 *On the uniqueness of weak solutions of Navier-Stokes equations: Remarks on a Clay Institute prize problem*
Johan Hoffman and Claes Johnson

2004–08 *A new approach to computational turbulence modeling*
Johan Hoffman and Claes Johnson

2004–09 *A posteriori error analysis of the boundary penalty method*
Kenneth Eriksson, Mats G. Larson, and Axel Mlqvist

2004–10 *A posteriori error analysis of stabilized finite element approximations of the helmholtz equation on unstructured grids*
Mats G. Larson and Axel Mlqvist

2004–11 *Adaptive variational multiscale methods based on a posteriori error estimation*
Mats G. Larson and Axel Mlqvist

2004–12 *Multi-adaptive Galerkin methods for ODEs V: Stiff problems*
Johan Jansson and Anders Logg

2004–13 *Algorithms for multi-adaptive time-stepping*
Johan Jansson and Anders Logg

2004–14 *Simulation of mechanical systems with individual time steps*
Johan Jansson and Anders Logg

2004–15 *Computational modeling of dynamical systems*
Johan Jansson, Claes Johnson, and Anders Logg

2004–16 *Adaptive variational multiscale methods based on a posteriori error estimation: Duality techniques for elliptic problems*
Mats G. Larson and Axel Mlqvist

2004–17 *Ultraconvergence of an interpolated finite element method for some fourth-order elliptic problems*
Andrey B. Andreev and Milena R. Racheva

2004–18 *Adaptive variational multiscale methods based on a posteriori error estimation: energy norm estimates for elliptic problems*
Mats G. Larson and Axel Mlqvist

2004–19 *Stabilized Lagrange multiplier methods for elastic contact with friction*
Per Heintz and Peter Hansbo

2005–01 *A posteriori error estimates for mixed finite element approximations of elliptic problems*
Mats G. Larson and Axel Mlqvist

2005–02 *On the numerical modeling of quasi-static crack growth in linear elastic fracture mechanics*
Per Heintz

2005–03 *Irreversibility in reversible systems I: the compressible Euler equations in 1d*
Johan Hoffman and Claes Johnson

2005–04 *Irreversibility in reversible systems II: the incompressible Euler equations*
Johan Hoffman and Claes Johnson

2005–05 *A Compiler for Variational Forms*
Robert C. Kirby and Anders Logg

2005–06 *Topological optimization of the evaluation of finite element matrices*
Robert C. Kirby, Anders Logg, L. Ridgway Scott and Andy R. Terrel

2005–07 *Modeling of resistive wall mode and its control in experiments and ITER*
Yueqiang Liu, M.S. Chu, A.M. Garofalo, Y. Gribov, M. Gryaznevich, T.C. Hender, D.F. Howell, R.J. La Haye, M. Okabayashi, S.D. Pinches, H. Reimerdes, P. de Vries, and EFDA-JET contributors

These preprints can be obtained from

www.phi.chalmers.se/preprints